Energy Conversion and Management 236 (2021) 114056

Contents lists available at ScienceDirect

Energy Conversion and Management

journal homepage: www.elsevier.com/locate/enconman

Globally scalable geothermal energy production through managed pressure operation control of deep closed-loop well systems

AmirHossein Fallah [a,*], Qifan Gu [a], Dongmei Chen [a], Pradeepkumar Ashok [a], Eric van Oort [a], Michael Holmes [b]

[a] The University of Texas at Austin, United States
[b] Eavor Technologies Inc., Canada

ARTICLE INFO

Keywords:
Deep closed-loop geothermal system (DCLGS)
Scalable power generation
Thermal-hydraulic modeling
Managed pressure operation (MPO)
Open-hole well completion

ABSTRACT

Closed-loop geothermal systems (CLGS) have been recently proposed as an alternative to the conventional enhanced geothermal system (EGS) concept to address many of the issues of concern with EGS, such as potential contamination of the circulating fluid and short-circuiting. Deep CLGS wells drilled in rock formations with in-situ temperatures above 200 °C could in theory be drilled anywhere around the world, thereby allowing for globally scalable geothermal energy production. A novel concept of integrating a managed pressure operation (MPO) system with deep CLGS (DCLGS) is presented here. The concept includes an open-hole completion of the lateral section, while the automatically controlled MPO system maintains wellbore integrity and avoids fluid contamination. A combined thermal and hydraulic model is also developed to demonstrate the feasibility of this concept. Using a robust semi-implicit numerical algorithm, the model can simulate the fast transients in a well, which enables the application of automated MPO control for real-time control of a DCLGS. Simulation results show that a 7 km deep U-shaped well with a 7 km open-hole lateral with a reservoir temperature of 250 °C can generate a thermal power of around 28 MW initially when the pump rate is set to 350 m^3/h. The results also show that casing of the lateral section has little impact on the outlet temperatures and thermal powers. An optimally insulated return section can increase the output power by 2%. The effect of pump rate is also studied. Even though the outlet temperature decreases, increasing the pump rate can improve the thermal power by 15%, when the pump rate is increased from 250 to 450 m^3/h.

1. Introduction

Geothermal energy is considered clean and renewable, and geothermal wells have been drilled and used for heat and electricity generation for many years [1–3]. However, the economical extraction of geothermal energy has been mostly limited to countries and regions with high subsurface temperature gradients (e.g. areas with active volcanism and tectonic activity) and permeable aquifers [4,5]. Conventional enhanced geothermal systems (EGS) require high rock porosity and permeability, sufficient fluid in place, and adequate fluid recharge, which are not always available [2,6]. Moreover, the direct contact between fluid and rock through fractures might cause problems such as fluid contamination, surface gas emissions, and induced seismicity [7–9]. To avoid these issues and to enable global scaling of geothermal energy generation, closed-loop geothermal systems (CLGS) were introduced [10]. A CLGS well essentially works as an indirect heat exchanger, where the circulating fluid absorbs energy from the rock formation as it flows through the well, eliminating the reliance on fractures and the associated issues observed in EGS wells.

Different CLGS designs have been proposed in the published literature [11]. These include pipe-and-annulus designs [12] and the U-shaped loops [13]. Abandoned oil and gas wells are also considered for geothermal energy production [14–16]. However, these existing concepts are mostly based on shallow wells and the estimated electricity generation in such wells is on the order of a few megawatts only, which may not be sufficient to generate electricity at a large utility scale (see e.g. Oldenburg et al. [17]). To generate commercially viable power at any location, deep CLGS (DCLGS) wells are required to enable access to high-temperature reservoirs. Taking the US as an example, a study by the Geothermal Laboratory at SMU [18] shows that geothermal reservoirs with temperatures above 200 °C at the depth of 7.5 km are available in

* Corresponding author.
E-mail addresses: afallah@utexas.edu (A. Fallah), qifan.gu@utexas.edu (Q. Gu), dmchen@me.utexas.edu (D. Chen), pradeepkumar@mail.utexas.edu (P. Ashok), vanoort@austin.utexas.edu (E. van Oort), mike.holmes@eavor.com (M. Holmes).

https://doi.org/10.1016/j.enconman.2021.114056
Received 30 September 2020; Accepted 11 March 2021
Available online 27 March 2021

Glossary

BHP	bottomhole pressure
CLGS	closed-loop geothermal system
DCLGS	deep closed-loop geothermal system
EGS	enhanced geothermal system
ERD	extended reach drilling
HPHT	high-pressure high-temperature
MD	measured depth
MPD	managed pressure drilling
MPO	managed pressure operation
PI	proportional integral
PVT	pressure–volume-temperature
SBP	surface backpressure
TVD	true vertical depth
VIT	vacuum insulated tubing

Nomenclature

A	cross sectional area, L^2, m^2
c_p	specific heat capacity at constant pressure, L^2/t^2T, J/Kg.K
c_v	specific heat capacity at constant volume, L^2/t^2T, J/Kg.K
D	diameter, L, m
e	internal energy, L^2/t^2, J/Kg
f_D	Darcy–Weisbach friction factor
f_g	gravitational force, m/L^2t^2, $Kg/m^2.s^2$
f_w	wall friction, m/L^2t^2, $Kg/m^2.s^2$
g	gravitational acceleration, L/t^2, m/s^2
h	convection heat transfer coefficient, $m/t^3.T$, $W/m^2.K$
H	enthalpy, L^2/t^2, J/Kg
$\dot{H}_{source}$	rate of enthalpy inlet from source/sink per unit volume, m/Lt^3, W/m^3
k	thermal conductivity, mL/t^3T, W/m.K
$\dot{m}_{source}$	rate of mass inlet from source/sink per unit volume, m/L^3t, $Kg/m^3.s$
$\dot{M}_{source}$	rate of momentum inlet from source/sink per unit volume, m/L^2t^2, $Kg/m^2.s^2$
Nu	Nusselt number
p	pressure, m/Lt^2, Pa
Pr	Prandtl number
$\dot{q}_{wall}$	rate of heat transfer from the wall per unit volume, m/Lt^3, W/m^3
r_i	inner radius, L, m
r_o	outer radius, L, m
R	thermal resistance, Lt^3T/m, $m^3.K/W$
Re	Reynolds number
t	time, t, s
T	temperature, T, K
v	velocity, L/t, m/s
x	length in direction of the well (measured depth), L, m
z	vertical position, L,m
μ	viscosity, Pa.s, Kg/m.s
ρ	density, m/L^3, Kg/m^3

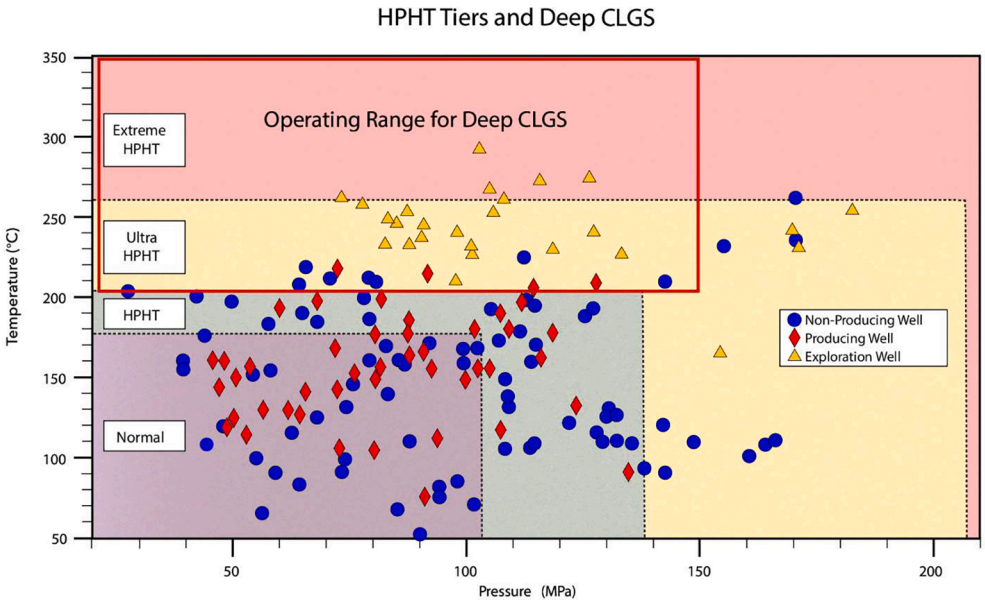

Fig. 1. HPHT tiers and operating range for deep CLGS wells (well information courtesy of Total, 2012 [24]). The box in red shows the operating range for deep CLGS wells considered here.

most regions within the US, most prominently in the western states and in south-east Texas. Thus, to access these reservoirs, it is necessary to drill wells that are deeper than existing wells.

Drilling deeper CLGS wells with longer lateral sections is technically difficult due to the extreme high-pressure, high-temperature (HPHT) conditions, the challenges associated with accurate directional drilling at depth, well integrity issues, etc. Technologies already developed in the oil and gas sector have the potential to meet these challenges and can be extended to deep geothermal drilling. Note that deep vertical wells have already been drilled up to 12 km true vertical depth (TVD). Two examples are the deep vertical wells drilled in Russia at the Kola Peninsula (12+ km) [19] and the KTB site in Germany (9+ km) [20]. Directional drilling techniques have also enabled drilling of very long horizontal sections [21,22]. Wells with total Measured Depths (MDs) of up to 15 km have been drilled using directional drilling and extended reach drilling (ERD) techniques [23]. As of 2012, multiple oil and gas exploration wells have been drilled in the operating range of the proposed deep CLGS, with in-situ temperature up to 290 °C (Fig. 1). In order

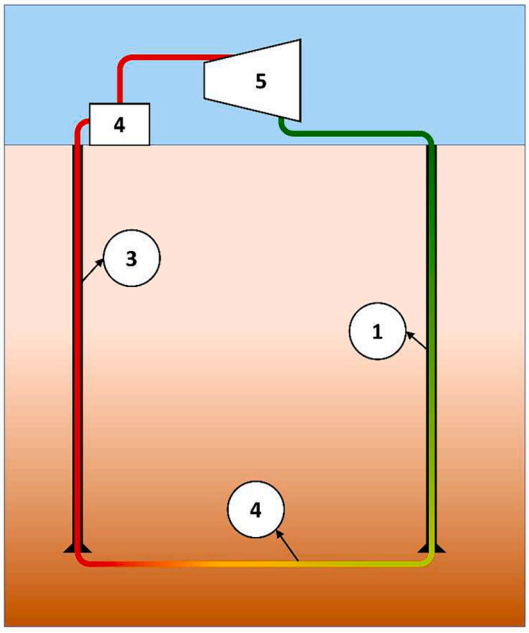

Fig. 2. Schematic of the MPO-controlled deep geothermal well concept, including (1) inlet section (cased), (2) lateral section (open-hole), (3) outlet section (cased or VIT-insulated), (4) MPO choke, and (5) turbine/heat exchanger.

to generalize the existing drilling techniques for deep wells and push the operation boundary into the red color circled zone of Fig. 1, it is necessary to develop a thorough understanding of the well hydraulics at depth and enable the development of transient behavior controller. As indicated below, the concept of CLGS is first introduced.

1.1. Deep CLGS concept introduction

Fig. 2 shows the concept of a DCLGS well with an integrated managed pressure operation (MPO) system. The geothermal well in this particular example is U-shaped and consists of two vertical wellbores. These wellbores are drilled to the desired temperature region (200+ °C) and connected by a long horizontal section (note that other DCLGS configurations are possible as well, but we are limiting the discussion here to a U-shaped well). This lateral section is preferably completed with an open-hole or "barefoot" completion, allowing for direct contact and efficient heat transfer between the fluid and the high-temperature rock. Moreover, an open-hole completion of the lateral section avoids practical problems with running casing and cementing downhole at extremely high temperatures. Due to the varying energy demand experienced by DCLGS wells and the frequent temperature cycling associated with operating, starting, and shutting down of the well, thermal expansion and contraction of the casing and maintaining integrity of the cement sheet may present major issues. Such problems are eliminated for the lateral section when it remains open to the formation as proposed by this study (note that the temperature cycling will still be an issue for the cased-hole sections of the well). For power generation, low-temperature working fluid is pumped into the well and is heated as it flows through the inlet vertical section of the well and the horizontal lateral section, absorbing energy from the surroundings. The outlet vertical section of the well could be thermally insulated to avoid heat loss to the formation when the high-temperature fluid returns to surface. An automatic MPO system, analogous to a managed pressure drilling (MPD) system used for the drilling of challenging oil and gas wells [25], is used to manage the pressure of the fluid flowing out of the exiting well. The MPO system will not only support the grid base load but also provide the load following capability that normally comes from the spin reserve. Using the MPO system to apply surface backpressure, it is possible to both control the pressure–volume-temperature (PVT) dynamics of the circulating fluid, as well as add additional hydrostatic pressure to maintain mechanical wellbore integrity in the lateral open-hole section. Moreover, by maintaining the pressure profile within the open-hole lateral section, the MPO system avoids reservoir influx into the wellbore (in case the reservoir rock is permeable) and eliminates fluid contamination issues. Finally, the energy is extracted from the high-temperature fluid in a turbine or heat exchanger, and the cooled fluid is re-injected into the wellbore.

To evaluate the feasibility of the integrated DCLGS with MPO concept as an economically viable power source and establish an analytical foundation for subsequent MPO control design, it is essential to first develop a thorough understanding of the hydraulic and thermal behavior of the fluid under the pertaining HPHT conditions of a DCLGS well. There are a few thermal models for the estimation of temperature profiles in U-shaped CLGSs in the published literature. Sun et al. [26] provides a literature review of U-shaped systems. Numerical models of Sun et al. [27] and Sun et al. [28] estimate the steady-state temperature profile in U-shaped wells using supercritical CO_2 as the working fluid. Schulz [10], Oldenburg et al. [17], and Song et al. [29] have developed models for simulating shallow U-shaped geothermal wells using water as the working fluid. These models can provide estimation of the temperature profiles over the lifetime of low-temperature CLGS wells. However, fast transients and short-term effects, such as those caused by changing the pump rate, are not considered in these models. Moreover, since capturing pressure wave behavior is required for dynamic well control, such models can only simulate cases where casing and heat conducting cement are used to seal off the horizontal section and wellbore stability is already ensured. In order to evaluate the feasibility of implementing DCLGS with commercial viability and to perform a subsequent control design, a transient dynamic thermal and hydraulic model is needed.

An integrated thermal and hydraulic model was developed to address this need and to evaluate the feasibility of the proposed DCLGS concept and ensure real-time MPO control. Details of this transient model development are presented in this paper, followed by a wide range of simulation scenarios that illustrate the potential of the DCLGS design under different conditions. Note that the lifetime performance of the geothermal system is beyond the scope of this paper. The long-time thermal depletion around the wellbore and the consequent power reduction can be estimated using external formation heat transfer models [30,31]. The main contributions of this paper are 1) introducing the concept of integrating an MPO control system with a deep CLGS well that enables access to high temperature reservoirs globally; 2) considering an open-hole completion of the lateral section for improved heat transfer and to avoid cementing issues at high temperature; 3) developing a transient model that can describe the highly coupled dynamic thermal and hydraulic behavior of the well to pave the way for MPO control design; and 4) enabling both base load support and transient load tracking to displace the spin reserve.

2. Thermal and hydraulic modeling

Our integrated thermal and hydraulic model to simulate DCLGS wells uses transient conservation equations to estimate different parameters, such as the dynamic temperature profiles and the generated power during the power generation phase. The model consists of one-dimensional conservation equations of the wellbore flow, an external heat transfer network between the wellbore flow and the rock formation, sub-models that calculate the properties of the water as functions of pressure and temperature, and a semi-implicit numerical scheme that solves the transient conservation equations. Details can be found in Fallah et al. [32,33], where an advanced thermal and multi-phase flow simulator was designed for kick simulations during oil and gas well drilling applications. The transient and steady-state results of the model

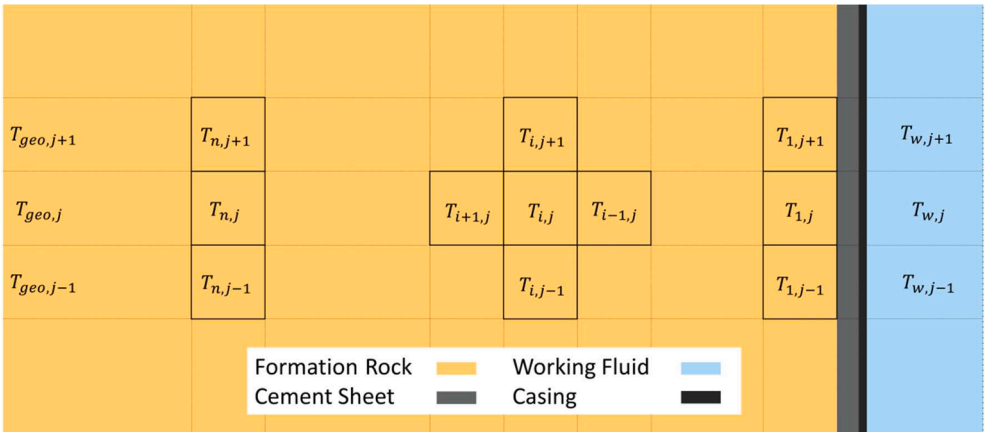

Fig. 3. Discretization of rock formation for heat transfer calculations for a cased section of the well (with bi-lateral symmetry). The casing and cement sheet are omitted when simulating open-hole well sections.

were validated against experimentally-validated analytical solvers [34] and commercial software [35], where a maximum discrepancy of 2 °C was observed. Results of the validation are provided in this paper (Appendix A. Model Validation). Note that in the proposed DCLGS concept, the MPO system controls the PVT behavior of the working fluid and avoids reservoir influx, reducing the flow to a single-phase liquid flow at all times. The modeling equations are briefly summarized below.

2.1. Conservation equations

The conservation equations of the entire system consist of a one-dimensional system of mass, momentum, and energy conservation equations to describe the water flow in the well (Eqs. (1)–(3)). The equations are derived from the transient Navier-Stokes equations for pipe flow and account for turbulent friction forces, liquid compressibility, and temperature-dependent water properties:

$$\frac{\partial \rho}{\partial t}+\frac{\partial \rho v}{\partial x}=\dot{m}_{source} \tag{1}$$

$$\frac{\partial \rho v}{\partial t}+\frac{\partial \rho v^2}{\partial x}=-\frac{\partial p}{\partial x}+f_g+f_w+\dot{M}_{source} \tag{2}$$

$$\frac{\partial \rho(e+\frac{1}{2}v^2+gz)}{\partial t}+\frac{\partial \rho v(h+\frac{1}{2}v^2+gz)}{\partial x}=\frac{\partial}{\partial x}\left(k\frac{\partial T}{\partial x}\right)+\dot{q}_{wall}+\dot{H}_{source} \tag{3}$$

where t is time, x is the length along the direction of the well (measured depth, MD), ρ is density, v is velocity, $\dot{m}_{source}$ is the rate of mass generation per unit volume from sources, p is pressure, f_g is gravitational force per unit volume, f_w is wall friction per unit volume, $\dot{M}_{source}$ is the rate of momentum generation per unit volume from sources, e is the internal energy, g is the gravitational acceleration, z is the vertical depth, h is enthalpy, k is thermal conductivity, T is temperature, $\dot{q}_{wall}$ is the rate of external heat transfer per unit volume through the walls, and $\dot{H}_{source}$ is the rate of enthalpy generation per unit volume from sources. Internal energy and enthalpy are defined as:

$$e=\int_{T_0}^{T} c_v(T)dT+e_0 \tag{4}$$

$$h=e+p/\rho \tag{5}$$

where c_v is the specific heat capacity at constant volume, and T_0 and e_0 are reference temperature and internal energy.

The two terms on the left-hand side of Eqs. (1)–(3) refer to the conservation and convective terms, respectively. The terms on the right-hand side are the source and sink terms for each equation. The rate of mass, momentum and energy generation from sources are calculated based on the transient flow rate and temperatures at the inlet and outlet of the well (e.g., pump inputs). The gravitational force and wall friction terms in the momentum equation are calculated as [36]:

$$f_g=\rho g\cos(\theta) \tag{6}$$

$$f_w=-\frac{1}{2}\frac{f_D\rho v^2}{D} \tag{7}$$

where θ is the hole deviation from the vertical direction, f_D is the Darcy–Weisbach friction factor (calculated from Ahmed and Miska [37]), and D is the hole diameter. The external heat transfer in the energy equation is calculated in the heat transfer network, discussed in the following.

The boundary conditions used to solve Eqs. (1)–(3) include the pump rate and inlet temperature at the wellbore inlet, as well as the wellbore outlet pressure which is enforced by the automated MPO system. The inlet pressure, output flow rate, and outlet temperature are calculated by the numerical scheme.

2.2. Heat transfer network

Heat transfer between the wellbore flow and the rock formation, which are separated by casing and cement for cased-hole sections and are in direct contact for open-hole sections, as well as inside the rock formation is calculated using the heat transfer network shown in Fig. 3. The rock formation is discretized radially to account for the formation temperature dynamics in close vicinity of the well. Due to the negligible temperature gradients in the axial direction, only the radial heat conduction inside the rock formation is taken into account [32]. The number of radial cells used to discretize the rock formation is changed automatically, such that the temperature change of the cell furthest from the well (the leftmost cell in Fig. 3) remains below a predefined threshold. Once the temperature change in the last cell exceeds the threshold, a new radial cell is added to the end of the heat transfer network. The dynamic discretization of the rock formation saves computational power by only discretizing the rock formation in the regions with significant temperature changes.

The heat transfer between the wellbore and the first formation node is calculated as:

$$\dot{q}_{wall}=\frac{T_1-T_w}{R} \tag{8}$$

where T_1 is the temperature of the first formation cell, T_w is the temperature of the water in the well, and R is the thermal resistance. Total thermal resistance is calculated by summing the individual resistances between the water and the first cell (i.e., convection in the water, con-

duction through the casing and cement (which is zero in open-hole), and conduction in the rock formation). The heat transfer between the adjacent formation cells is calculated similarly, where the resistance is only the conduction resistance through the rock. Each individual conduction or convection resistance is calculated as:

$$R_{conduction} = \frac{A ln\left(\frac{r_o}{r_i}\right)}{2\pi k_s} \tag{9}$$

$$R_{convection} = \frac{A}{h\pi D} \tag{10}$$

where A is the cross-sectional area of the well, r_o and r_i are the outer and inner radius of the solid across which heat is being conducted, k_s is the conductivity of the solid, D is the diameter of the wall at which heat is being convected, and h is the convection coefficient. The convection coefficient is defined as:

$$h = \frac{Nuk}{D} \tag{11}$$

where k is the conductivity of water, D is the diameter of the hole, and Nu is the Nusselt number calculated from Eq. (12) [38]:

$$Nu = \begin{cases} 4, & laminar\ flow \\ \dfrac{\left(\frac{f}{8}\right)(Re-1000)Pr}{1+12.7\left(Pr^{\frac{2}{3}}-1\right)\sqrt{\frac{f}{8}}}, & turbulent\ flow \end{cases} \tag{12}$$

where Re and Pr are the Reynolds number and Prandtl number, respectively.

2.3. Water properties

In a first approach, we assume that water is used as the circulation fluid. This is not a restriction of DCLGS wells, and other working fluids such as supercritical CO_2 can also be considered. Due to the extreme pressure and temperature conditions in the DCLGS well, assuming constant properties will lead to large errors. Water viscosity, for example, decreases by a factor of 18 from 0 °C to 300 °C. Therefore, fitted polynomial models of water properties are used to calculate the density, viscosity, specific heat capacity at constant pressure and constant volume, and thermal conductivity [39,40]. Density is modeled by a first-order polynomial function of pressure combined with a second-order polynomial function of temperature as:

$$\rho = \frac{p}{1490.9} - 0.0026*T^2 - 0.1594*T + 1001.5515 \tag{13}$$

where pressure is measured in Pa, temperature in °C, and density in kg/m^3.

Neglecting the effect of pressure, the viscosity, specific heat capacities, and thermal conductivity are assumed to be functions of temperature and are modeled as:

$$\mu = \begin{cases} 3.27*10^{-11}*T^4 - 9.14*10^{-9}*T^3 + 9.93*10^{-7}*T^2 - 5.56*10^{-5}*T + 1.79*10^{-3}, & T < 100\ ^\circ C \\ -2.025*10^{-11}*T^3 + 1.72*10^{-8}*T^2 - 5.18*10^{-6}*T + 6.44*10^{-4}, & T \geq 100\ ^\circ C \end{cases} \tag{14}$$

$$c_p = 1.16*10^{-4}*T^3 - 2.35*10^{-2}*T^2 + 1.61*T + 4.17*10^3 \tag{15}$$

$$c_v = 3.40*10^{-5}*T^3 - 1.01*10^{-2}*T^2 - 3.95*T + 4.24*10^3 \tag{16}$$

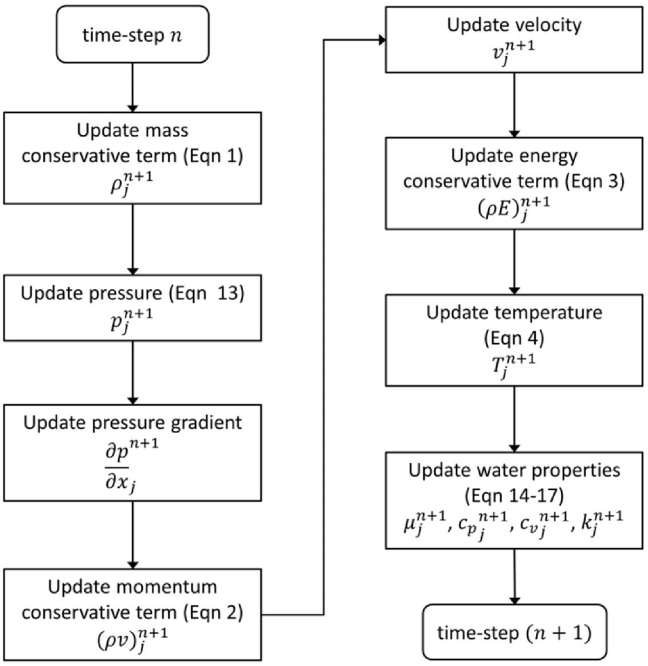

Fig. 4. Solution procedure of the semi-implicit numerical scheme at each time-step.

$$k = -5.71*10^{-6}*T^2 + 1.64*10^{-3}*T + 5.69*10^{-1} \tag{17}$$

where temperature is measured in °C, viscosity in Pa.s, specific heat capacities in J/Kg.K, and thermal conductivity in W/m.K.

2.4. Numerical scheme

To solve the conservation equations, the wellbore is discretized in the axial direction. A semi-implicit numerical scheme is used to enable real-time simulations. Details of the semi-implicit numerical scheme and the discretization of Eqs. (1)–(3), as well as the validation of the discretization method are provided by Evje and Fjelde [41]. Using small time-steps on the order of 10^{-3} s (with a mesh size of 25 m), the model captures the pressure waves in the water column, which is necessary for operating the automatic controller that maintains the surface back-pressure. The time-step and mesh size are selected such that the solution is stable, accurate, and independent of the selected time-step and mesh size. Fig. 4 shows a flowchart of the computational scheme used by the model. The subscripts and superscripts in the figure refer to the cell number and time-step, respectively. First, the mass conservation equation and the density model are used to obtain the density and pressure at each new time-step. Using the updated pressure, the pressure gradient term in the momentum equation is calculated (implicitly). The implicit calculation of the pressure gradient guarantees the numerical stability of the software [41]. Subsequently, velocity and temperature are updated using the momentum and energy conservation equations, respectively.

The energy equation is assumed to be de-coupled from the mass and momentum equations since the temperature dynamics are much slower than the mass dynamics. Finally, the properties of the water and source/sink terms in Eqs. (1)–(3) are updated for the next time-step.

2.5. Automated choke control

Due to the high temperatures in the well, water will boil as it is being circulated back to surface. Large differences between the densities of liquid water and water vapor lead to a large drop in hydrostatic pressure. This change in pressure makes control over the bottomhole pressure (BHP) and maintaining well integrity (in the case of an open-hole completion) challenging. Reservoir fluids could also enter the well (through any exposed permeable formations and fractures) and pollute the water that is circulated out of the well. Moreover, evaporation could lead to excessive pressures on surface due to the expansion, resulting in safety hazards and risks and compromising wellbore integrity control. To address these issues and control the water's PVT behavior, return flow is controlled using an automatic choke such that the entire operation is under MPO control at any time. The proposed MPD system is analogous to the MPD system used in the oil and gas industry (Appendix B. Managed Pressure Operation). A polynomial fit of the pressure as a function of temperature is presented in Eq. (18). The boiling pressure monotonically increases with the temperature [39]. At any given temperature, water starts boiling if the pressure is below the boiling pressure threshold.

$$p_{boil} = 1.57*10^{-3}*T^4 - 2.44*10^{-1}*T^3 + 3.30*10^{1}*T^2 - 1.77*10^{3}*T + 3.46*10^{4} \quad (18)$$

In Eq. (18), temperature is measured in °C and pressure in Pa. Deep in the wellbore itself, the hydrostatic pressure of the water column applies sufficient pressure to avoid boiling downhole, even for extreme temperature gradients and high absolute downhole temperatures. The well location where boiling is most likely to occur is on surface at the outlet (see Fig. 3) due to the reduced hydrostatic pressure. Therefore, a proportional integral (PI) controller that enables MPO was designed to maintain a surface backpressure (SBP) above the boiling pressure by adjusting the choke opening automatically. Note that the MPO system plays a crucial role in the proposed DCLGS concept. The MPO system controls the fluid PVT behavior, maintains pressure control across the open lateral, ensures well integrity, and avoids reservoir influxes and fluid contamination. Simulating the automated choke control behavior relies on capturing the pressure wave dynamics and the fast transients associated with rapid choke adjustments. In this paper, we simulate choke opening manipulation such that:

$$p_{surface} = p_{boil}(T) + SM \quad (19)$$

where $p_{surface}$ is the SBP that is maintained by the choke, p_{boil} is the boiling pressure on surface (which is a function of the outlet temperature), and SM is an additional safety margin that may also account for excess pressure needed for maintaining wellbore stability in exposed open-hole sections in the well (note that this term can be further delineated if real-time estimation of pore pressure and the pressure requirements for wellbore stability is possible, see e.g. Zoback [42]). Temperature data collected at a one-minute-or-higher frequency are used in the model to calculate the boiling pressure and maintain the required SBP. For the simulations presented here, the safety margin is set to 1 MPa.

3. Simulation scenarios

To demonstrate the utility of the model in simulating the operation and well control of DCLGS wells, two cases with different geometries are discussed here. In both cases, water is pumped at 300 m^3/h into a U-shaped well for 13 h, followed by a 3-hour pumping at 400 m^3/h, and 4 h of pumping at 350 m^3/h. The simulated scenario shows how the dynamic temperature and generated power change with the changes of the pump rate. The first well consists of two 7 km deep vertical sections (which would be drilled independently) that are connected through a 7 km horizontal section (which could be drilled as two 3.5 km sections drilled from the two independent wells that intersect at their endpoints), referred to as the "7/7" geometry. The wellbore diameter in the open-hole lateral section is assumed to be 31.115 cm (12.25 in, in line with industry standard production hole diameters in oil and gas wells) and the build radius of the curve sections of the well is assumed to be 200 m. The initial temperature of the water in the well is assumed to be equal to the temperature profile of the surrounding rock, linearly increasing from 40 °C at surface to 250 °C at 7 km TVD (a temperature that is observed at this vertical depth in locations such as the Los Angeles metropolitan area [18]). The second well has a TVD of 10 km with a 5 km lateral section, referred to as the "10/5" geometry. The geothermal temperature gradient with depth is assumed to be constant and the same for the two geometries, leading to a bottomhole temperature of 340 °C for the "10/5" geometry. For both geometries, the density, heat capacity, and thermal conductivity of the rock formation are set to be 2700 kg/m^3, 1000 J/kg.K, and 2.5 W/m.K, respectively. These values represent average crust properties [43]. While these values depend on the rock formation, they do not vary significantly among different rock types [44]. Hence, for different sets of formation properties, the resulted output temperature and generated thermal power behavior are similar with small variations. Table 1 provides the parameters used in the simulations. In these case studies, water is pumped continuously for 20 h. During the simulation, the automatic controller is used to apply enough backpressure to avoid water evaporation and associated pressure reduction in the wells. The inlet and outlet vertical sections use 33.973 cm (13.375 in) outer diameter casing. Casing and cement thicknesses for the cased sections are set to be 1 cm and 2.5 cm, respectively.

Table 1
Relevant geometrical, formation, fluid and geothermal parameters used in the simulations.

Geometry		**Fluid Properties**	
Vertical depth	7000/10000 m	Working fluid	Water
Horizontal length	7000/5000 m	Density	Eq. (13)
Build radius	200 m	Viscosity	Eq. (14)
Hole size (open-hole)	31.115 cm	Specific heat capacities	Eq. (15) and (16)
Hole size (casing)	31.788 cm	Thermal conductivity	Eq. (17)
Casing/cement thickness	1 cm/2.5 cm	**Formation Properties**	
Geothermal Temperature		Density	2700 kg/m^3
Downhole temperature	250/340 °C	Heat capacity	1000 J/kg.K
Temperature gradient	0.03 °C/m	Thermal conductivity	2.5 W/m.K

Figs. 5 and 6 show the water, rock formation (first node), and initial temperatures versus MD at different times into the simulation for the "7/7" and "10/5" geometries, respectively. Water temperature is initially assumed to be in thermal equilibrium with the rock formation (e.g., after an extended shut-in period of no circulation). When pumping starts, high-temperature water in the horizontal section is pumped out of the well and replaced by cold water from the inlet section of the well. After continuing pumping for a few hours, a semi-steady-state is reached in which all the water is displaced by the cold water from the inlet section of the well. During the process, the surrounding rock temperature continues to decrease due to the heat transfer to the water (i.e., thermal depletion of the well). As the water is circulated up in the return section, the temperature of the surrounding rock drops, causing a heat loss from the water to the cold rock formation near surface. The maximum gradient in the temperature profile is observed at the beginning of the horizontal section, where the temperature difference between the water and un-cased formation is at a maximum. It is observed that the increased pump rate between 13 and 16 h into the simulation reduces the temperature profile along the well. This is because with the

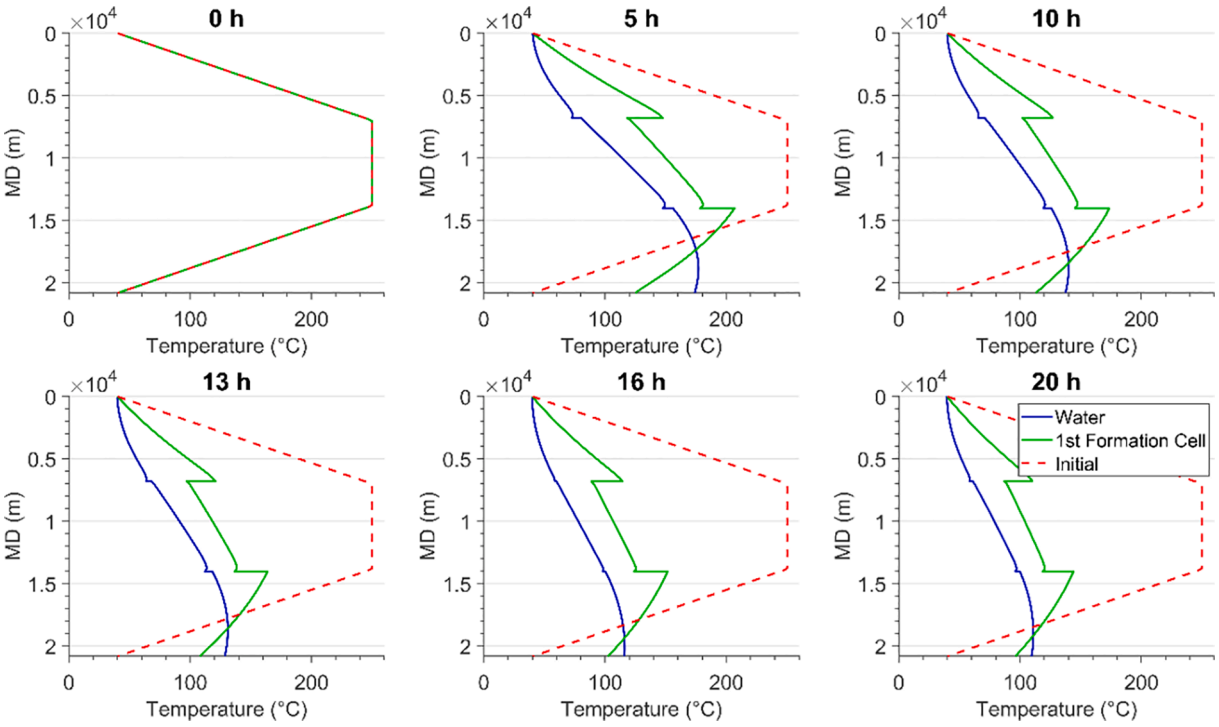

Fig. 5. Temperature profile at different times for the "7/7" geometry (with open-hole lateral).

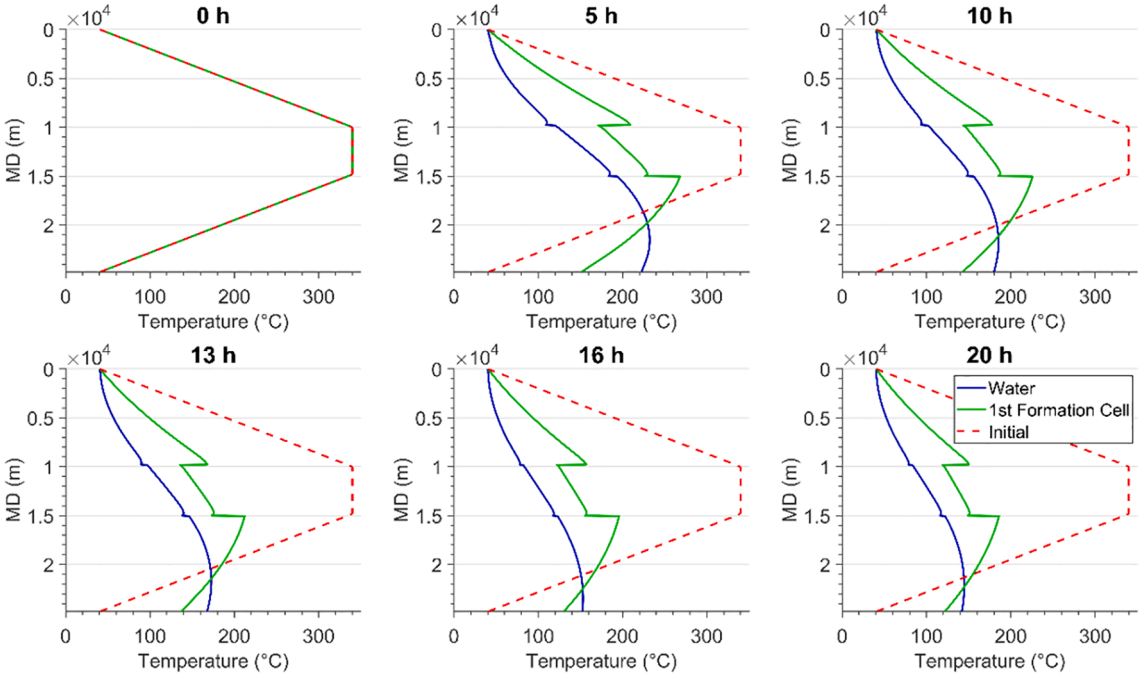

Fig. 6. Temperature profile at different times for the "10/5" geometry (with open-hole lateral).

increased pump rate and fluid velocities within the wellbore, water has less time to be heated up as it moves along the well.

In the lateral section, water temperature increases along the well direction due to the heat transfer with the formation at 250 °C or 340 °C for the "7/7" and "10/5" geometries, respectively. The temperature gradient along this section slowly decreases as the water and formation temperatures increase towards the geothermal temperature, reducing the temperature difference (cf. Figs. 5 and 6). Theoretically, in an infinitely long lateral section, water temperature will reach the maximum possible downhole temperature, which is equal to the undisturbed in-situ formation temperature. However, as the lateral length increases, the total cost and complexity of drilling increases, while the gain in power generation declines. Therefore, there exists an optimum lateral length beyond which the gain in power generation does not compensate for the extra cost of drilling. This optimum length depends on other parameters as well, most importantly the TVD (or equivalently, the maximum geothermal temperature reached), the pump rate, and the hole size. The developed model can be used to determine the optimum

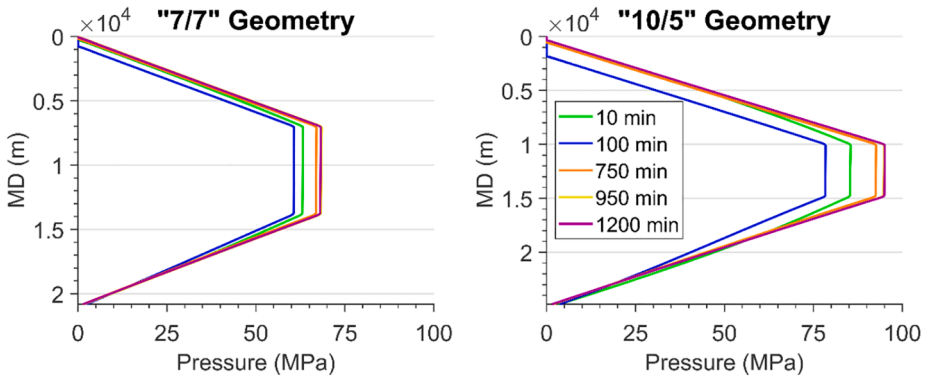

Fig. 7. Pressure profile at different times for geometries (with open-hole lateral).

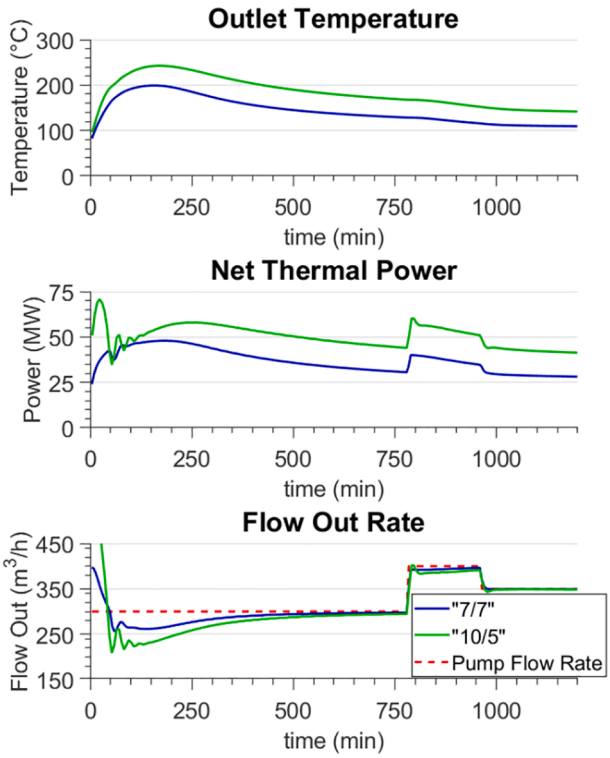

Fig. 8. Outlet temperature, thermal power and outlet flow versus time for both geometries (with open-hole lateral).

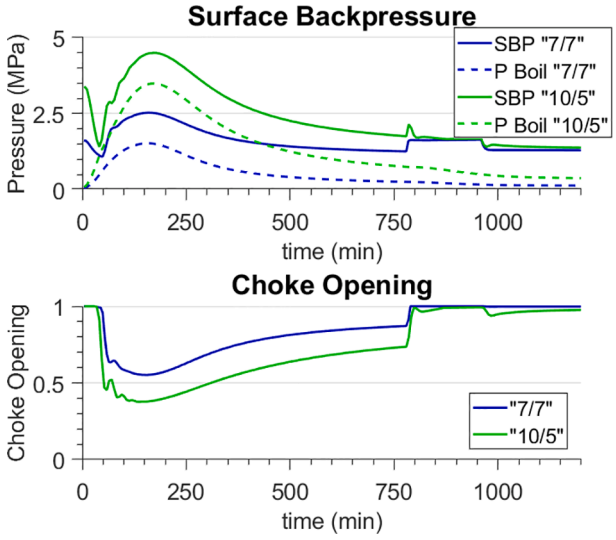

Fig. 9. SBP and choke opening versus time for both geometries (with open-hole lateral).

well geometry and pump rate for well design and efficient power generation for a given set of subsurface pressure and temperature conditions.

Fig. 7 shows the pressure profile at different times for both geometries. The pressure profile is affected by the hydrostatic pressure, frictional pressure drop, and SBP. While the pressure is mostly determined by the hydrostatic pressure, a small pressure drop is observed in the horizontal section due to friction for both geometries. At around 100 min, hot water that was initially in the well reaches surface and SBP is increased due to the higher outlet temperature, requiring a higher pressure to avoid boiling. At this time, because of the high temperature difference between the inlet and outlet sections of the well, the density and hydrostatic pressure in the outlet section of the well reduces, resulting in a lower BHP. The higher hydrostatic pressure gradient in the inlet section of the well results in a zero pumping pressure, a situation known as the thermosiphon effect [45], which reduces the power demand of the pumps. The thermosiphon effect is reduced as the temperature in the outlet section of the well decreases towards the steady-state temperature. With the changes in pump rate (at 13 h and 16 h into the simulation), the frictional pressure drops along the well changes. It is observed that the increased pump rate of 400 m^3/h at 950 min into the simulation results in a higher BHP compared to the BHP at 1200 min (350 m^3/h) and 750 min (300 m^3/h). The BHP changes need to be accounted for when determining the required SBP for well control over the open-hole lateral section.

Fig. 8 shows DCLGS outlet temperature, the net thermal power generation, and the outlet flow rate for both geometries while the pumping rate begins at 300 m^3/h, increases to 450 m^3/h between 780 and 960 min, and reduces to 350 m^3/h after 960 min. It is noted that the power values do not include any losses at surface due to power conversion in e.g., steam turbines: the numbers reflect the net thermal power that is generated by the producing well only. While the pump flow rate is kept at 300 m^3/h for the first 780 min into the simulation, oscillations are observed in the outlet flow rate during the early stages of power generation. These variations are mainly caused by the compression and expansion of the water due to pressure changes in the well (Fig. 7), as well as the thermal expansion behavior of the water within the wellbore. During the first 50 min, the hydrostatic pressure decreases due to the elevated temperatures in the return section of the well. This causes water expansion in the well and increases the outlet flow rate. At

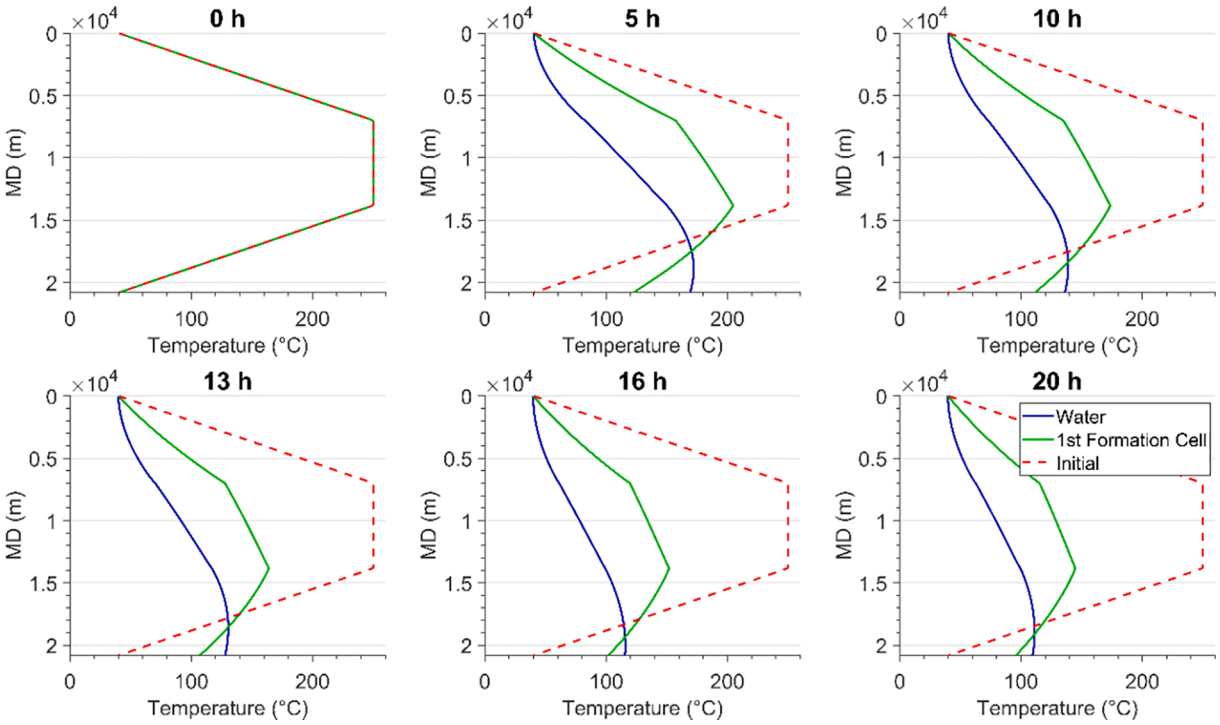

Fig. 10. Temperature profile at different times for the "7/7" geometry (with cased lateral).

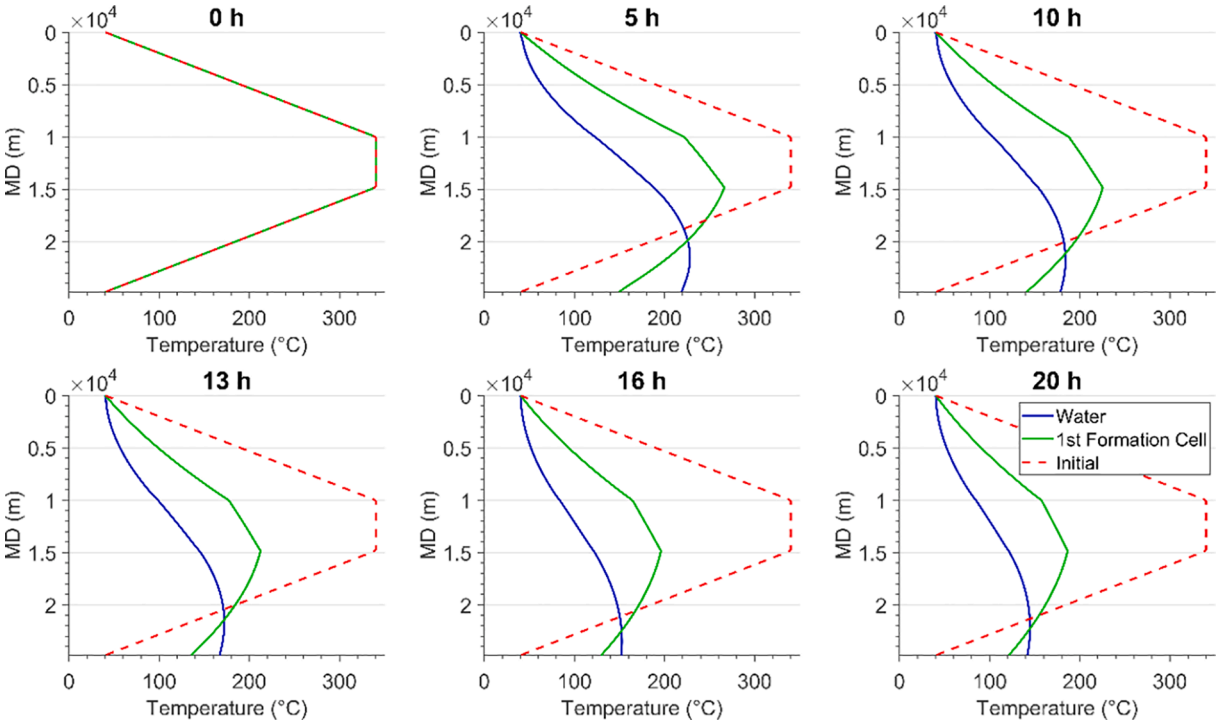

Fig. 11. Temperature profile at different times for the "10/5" geometry (with cased lateral).

50 min, the MPO system starts to increase the surface backpressure to avoid evaporation. Due to the increased backpressure and the resulting compression of the water, the outlet flow rate is decreased after this time. As steady-state approaches, the outlet flow rate converges to the pump rate value. When the inlet pump rate changes at 780 and 960 minutes, the outlet flow rate converges to the inlet pump rate and the wellbore reaches steady-state again.

The generated thermal power depends on the outlet temperature and outlet flow rate. During the initial stages of circulation, the high-temperature water that initially stays at bottomhole is circulated towards surface, increasing the outlet temperatures and the resulting thermal powers. Thereafter, the temperature and power slowly decrease with time due to the cooling of the heat-supplying rock, with some variations in the generated power caused by the varying outlet flow rate. At 780 min (300 m^3/h), the outlet temperature and net thermal power for the "7/7" geometry are 128 °C and 30.6 MW (168 °C and 44.0 MW

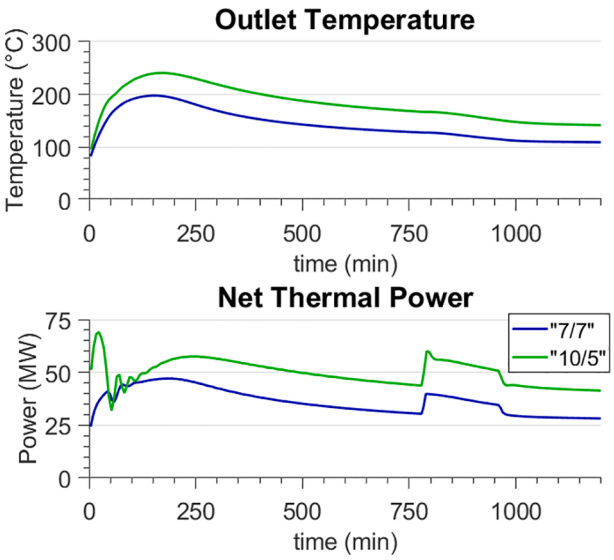

Fig. 12. Outlet temperature and thermal power versus time for both geometries (with cased lateral).

for the "10/5" geometry). With the pump rate increasing at 780 min, the net thermal power is increased to 40.0 and 60.2 MW for the "7/7" and "10/5" geometries, respectively. However, as the higher pump rate is maintained, the outlet temperature slowly decreases due to the reduced heat transfer time, thus reducing the generated thermal power. At 960 min, the pump rate drops to 350 m^3/h, which reduces the net thermal power. However, as the circulation is continued, wellbore temperatures are recovered due to the improved heat transfer time at lower fluid velocities, increasing the outlet temperature and thermal power. At 1200 min, the outlet temperature is 109 °C and the resulting net thermal power is 28.1 MW for the "7/7" geometry. (142 °C and 41.4 MW for the "10/5" geometry).

Fig. 9 shows the SBP and choke opening versus time. As the outlet temperature increases between 0 and 170 min (Fig. 8), the boiling pressure increases according to Equation (18). The automated controller calculates the boiling pressure, adjusts the choke opening, and applies sufficient SBP to avoid evaporation and maintain well control. A maximum SBP of 2.5 MPa and 4.5 MPa is applied at 75 min for the "7/7" and "10/5" geometries, respectively. As the temperature and boiling pressure decrease, the choke is slowly opened to reduce the excessive SBP, while maintaining a safety margin of 1 MPa (assuming in this case that no excess safety margin is needed for open-hole stability control in the horizontal lateral). Varying the pump rate will affect the outlet temperature, and the choke is automatically adjusted to maintain the 1 MPa safety margin while the boiling pressures vary.

3.1. *Effect of cementing the lateral section*

While cementing and casing problems can be avoided through open-hole completion of the lateral, it may not always be feasible to drill and maintain long open-hole lateral sections. In this case, the lateral section

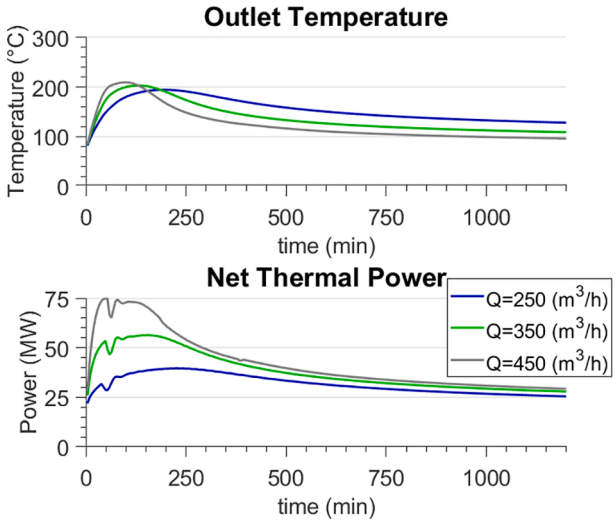

Fig. 14. Comparison of the outlet temperature and the generated power for different pump rates.

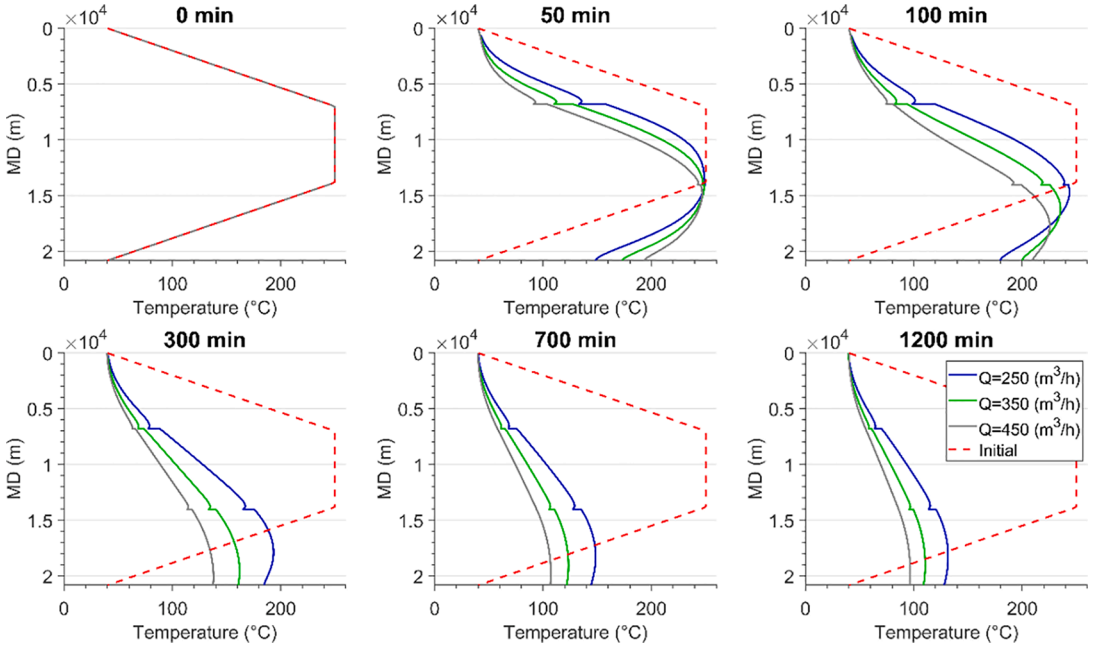

Fig. 13. Comparison of the temperature profiles for different pump rates.

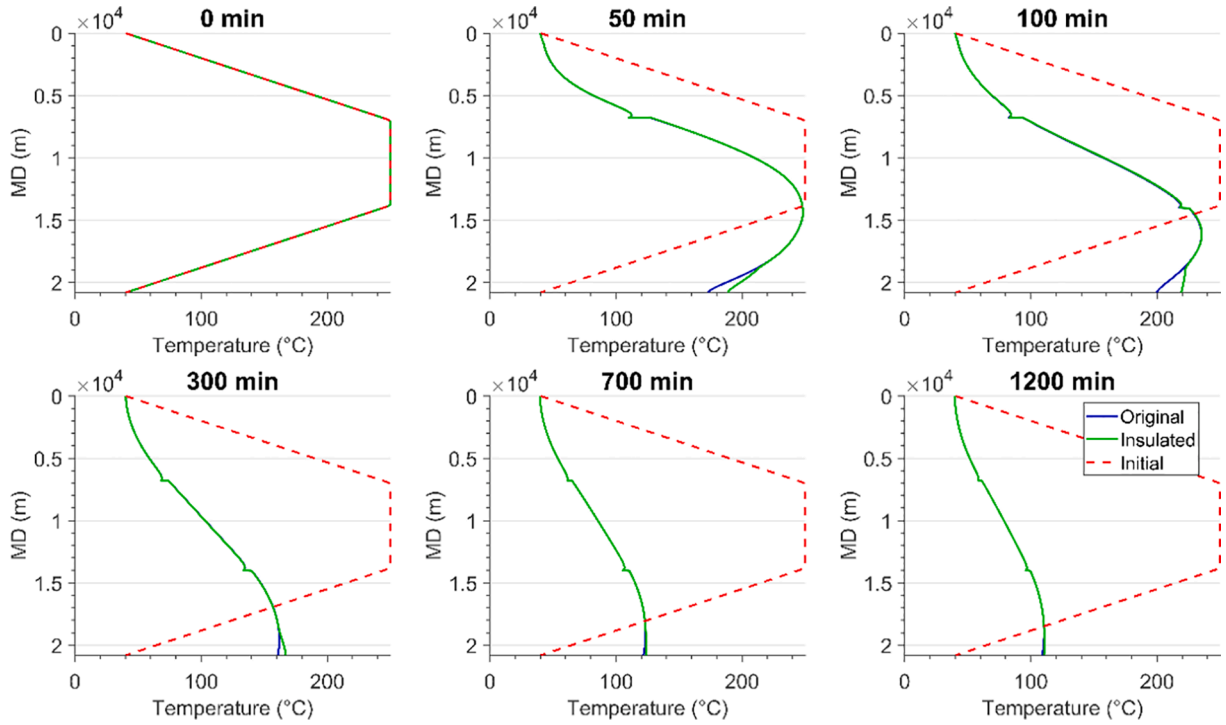

Fig. 15. Comparison of temperature profiles for uninsulated versus insulated wellbores.

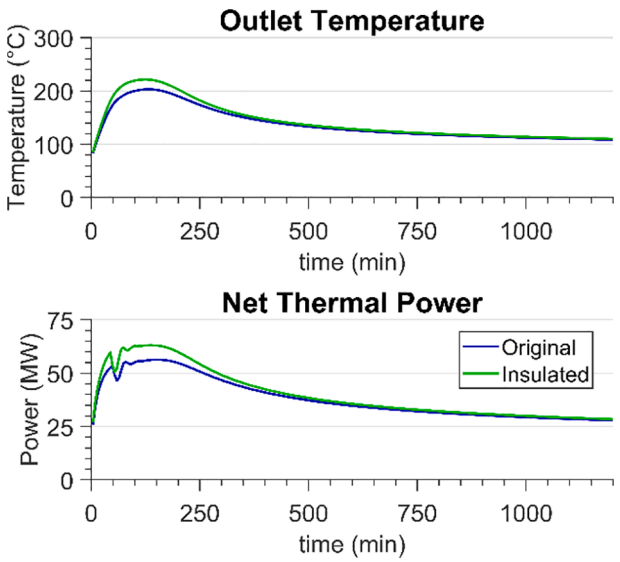

Fig. 16. Comparison of the outlet temperature and the generated power for uninsulated versus insulated wellbores.

needs to be cased and cemented to ensure wellbore integrity. Figs. 10–12 show the temperature profiles and the generated thermal power for cased lateral sections for both geometries. The outlet temperatures at 1200 min (where the pump rate is 350 m^3/h) are 110 °C and 142 °C for the "7/7" and "10/5" geometries, respectively. The outlet temperatures result in net thermal powers of 28.2 MW and 41.4 MW for the "7/7" and "10/5" geometries, respectively. These values are similar to the cases with open-hole lateral, showing that the heat transfer is mostly limited by the slow heat conduction in the rock formation.

3.2. *Effect of pump rate*

For a given well geometry, the generated power can be controlled by adjusting the pump rate. In this section, the effects of three different pump rates (i.e., 250, 350, and 450 m^3/h) on the power generation of the "7/7" well geometry are compared. In each case, the pump rate is maintained for 20 h until steady-state is reached. Fig. 13 shows the water temperature profile of the three different pump rates. The higher flow rate for the case of 450 m^3/h pump rate results in a lower output temperature compared to the other two cases with lower pump rates. This is because at higher pump rates, the water has less time flowing through the inlet and lateral sections, thus less time to absorb the heat from the surrounding formation. Fig. 14 shows the outlet temperature and the net thermal power during the first 20 h of pumping. The maximum outlet temperature is reached at 194, 132 and 99 min for the 250, 350 and 450 m^3/h cases, respectively. The outlet temperatures at 1200 min are 128, 109 and 96 °C for the three cases, correspondingly. It should be noted that the generated power slightly increases with the rising pump rate despite a lower outlet temperature. This is due to the increased mass flow rate through the well which carries more thermal energy per unit time to the surface and compensates for the lower output temperature. After 1200 min, the generated thermal powers of the 250, 350 and 450 m^3/h cases are 25.5, 27.9 and 29.3 MW, respectively. Varying pump rate, and associated SBP changes controlled by the MPO system, is therefore an effective way to deal with an ever-changing commercial power demand, which can also reduce the thermal depletion and improve the life-time performance of the well.

3.3. *VIT insulation effect*

Figs. 15 and 16 show the effect of insulating the outlet section of the well using VIT. In this section, the geometry of the "7/7" geometry is used with a constant pump rate of 350 m^3/h. Two cases are compared: (1) using a conventional casing string and cement sheet similar to the inlet section of the well (referred to as the "original case") and (2) insulating the near surface parts of the return section of the well where

the rock temperature is lower than the fluid temperature (referred to as the "insulated case"). In this case, the optimum insulated depth is 2 km, where the remaining parts of the return section are cased and cemented.

Fig. 15 shows the temperature profile of the two cases at different times. Temperature profiles are similar along the inlet and lateral sections of the well for both cases due to the same external conditions. However, the heat loss to the near-surface surrounding rock in the original case results in a temperature drop along the top 2 km of the outlet section of the well. This effect is more pronounced at around 100 min due to the larger temperature difference between the water and the rock formation behind the cement sheet, resulting in more heat loss. At 1200 min, a temperature drop of about 2 ℃ is observed in this case, while the temperature in the outlet section of the well near surface for the insulated case remains relatively unchanged. This effect would be more pronounced in deeper wells that produce higher outlet temperatures.

Fig. 16 compares the outlet temperature and thermal power generation for the two cases. At 1200 min, the thermal power of the insulated case is about 0.6 MW higher than that of the non-insulated case, indicating the importance of insulating the outlet section of the well. The maximum observed surface temperature is 221 °C and 203 °C for the insulated case and the original case, respectively.

4. Conclusions

A novel concept of integrating an automated managed pressure operation (MPO) system with a deep closed-loop geothermal system (DCLGS) for scalable power generation is introduced in this paper. Compared to existing closed-loop designs, the proposed concept considers wells at large well depth to access formations at 200 °C−350 °C in-situ temperature and includes an open-hole lateral section to avoid casing expansion/contraction and cement integrity issues at high temperature conditions. The proposed MPO system applies the required backpressure through an automatically controlled choke placed at the well outlet to ensure real-time wellbore integrity over the open-hole lateral region and control the phase behavior of the circulating fluid.

To demonstrate the concept's feasibility, a combined thermal and hydraulic model was developed to describe the transient well hydraulics during the operation and production stages of the DCLGS. Compared to existing models in the literature, the proposed model uses a fully-transient semi-implicit algorithm that can capture the pressure waves and fast transients, which are necessary for MPO control. The model can predict the generated thermal power for operation scenario with various true vertical well depth and horizontal length, open-hole or cased-hole lateral completions, heat insulation or lack thereof of the return flow, and changing pump rates. Simulation results show that the proposed integrated DCLGS concept with wells drilled in temperature environments above 200 °C can initially generate net thermal power in the range of 25–50 MW for a wellbore of 31.115 cm diameter and a circulating flow rate in the range of 300–400 m^3/h. The MPO control will enable geothermal wells to support the base load as well as displace the spin reserve.

Simulation results reveal that optimized thermal insulation of the return flow near surface could improve the power generation of the DCLGS well. Casing and cementing of the lateral section (e.g., when necessary for well control and to avoid influx) does not significantly affect the thermal performance of the well, which is due to the relatively small thickness of cement and casing layers. It was also observed that while increasing the pump rate reduces the outlet temperature, the generated thermal power could be increased by 15%. The maximum power generation can be achieved by optimally control the flow rate such that the energy exchange is maximized.

CRediT authorship contribution statement

AmirHossein Fallah: Conceptualization, Methodology, Software, Validation, Formal analysis, Writing - original draft, Visualization. **Qifan Gu:** Methodology, Software. **Dongmei Chen:** Conceptualization, Methodology, Writing - review & editing, Supervision. **Pradeepkumar Ashok:** Conceptualization, Methodology, Writing - review & editing, Supervision. **Eric van Oort:** Conceptualization, Methodology, Writing - review & editing, Supervision, Project administration, Funding acquisition. **Michael Holmes:** Methodology, Validation.

Declaration of Competing Interest

The authors declare that they have no known competing financial interests or personal relationships that could have appeared to influence the work reported in this paper.

Acknowledgements

The authors would like to thank the members of the Rig Automation and Performance Improvement in Drilling (RAPID) group at The University of Texas at Austin, United States for the financial support provided for this project.

Appendix A. Model validation

In this appendix the validation results of the thermal model against experimentally-validated models are provided for reference. More details and the parameters used in the validation case can be found elsewhere [33]. Since there is a distinct lack of reliable temperature data from test wells and actual wells in the field, the temperature results of the model are compared against the single-phase steady-state analytical solver of Hasan and Kabir [34] as well as a transient commercial software that is based on the hydraulic model of Petersen et al. [35].

The validation case consists of pumping drilling mud at a constant rate of 26.12 m^3/h and 26.7 °C into a 4200-m vertical well. Temperature profiles of the drillstring and annulus fluids are compared in Fig. A1. Results show a great match between the developed model and the validation models, with a maximum temperature discrepancy of 2 °C at the bottom of the wellbore. The difference can be attributed to the different density models used in each model. However, aside from the

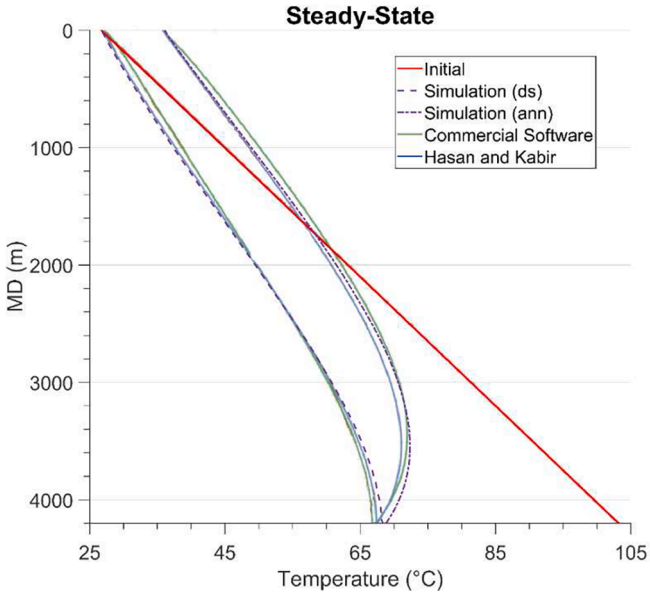

Fig. A1. Steady-state temperature profiles (from Fallah et al. [33]).

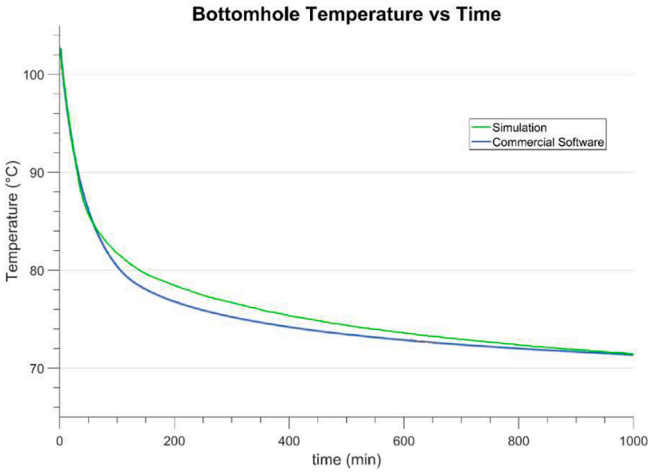

Fig. A2. Bottomhole temperature versus time (from Fallah et al. [33]).

small deviations, the comparisons show a good match both for the drillstring and annulus temperatures.

Fig. A2 shows the bottomhole temperature versus time for the developed model and commercial software (note that the Hasan and Kabir model is a steady-state solver and cannot predict transient effects). The maximum discrepancy is 2 °C, which is observed at 200 min into the simulation.

Appendix B. Managed pressure operation

The automated managed pressure operation (MPO) system proposed in this paper is analogous to the managed pressure drilling (MPD) system used in the oil and gas industry to drill challenging wells. The MPD system consists of a choke (that is preferably automated) on the outlet side of the wellbore. By adjusting the choke opening, the amount of backpressure can be adjusted to control the pressure at the bottomhole (or the entire open-hole section). In oil and gas, MPD systems are used to maintain the bottomhole pressure (BHP) within tight drilling margins and avoid/control reservoir influx [46–48]. Fig. B1 shows the performance of an automated MPD system in controlling the BHP after a gas influx [36].

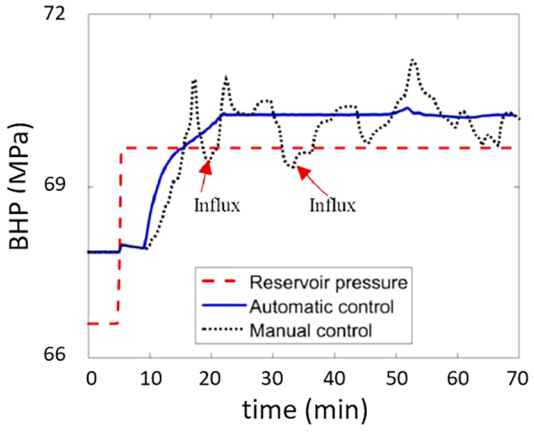

Fig. B1. Performance of automated MPD in controlling the BHP. (courtesy of Ma et al. [36]).

The same concept could be implemented for the proposed deep closed-loop geothermal system (DCLGS) concept. The MPO system will (1) maintain the pressure within the open-hole region to avoid any reservoir influx and fluid contamination and to ensure wellbore stability; and (2) control the phase behavior of the working fluid by ensuring the downhole or pipe pressure is above the evaporation pressure in real-time.

References

[1] Watson A. Geothermal engineering. New York: Springer-Verlag; 2016.
[2] Tester J, Anderson B, Batchelor A, Blackwell D, DiPippo R, Drake R, et al. The future of geothermal energy. Massachusetts Inst Technol 2006:358.
[3] Tester J, Blackwell D, Petty S, Richards M, Moore M, Anderson B, et al. The future of geothermal energy: an assessment of the energy supply potential of engineered geothermal systems (EGS) for the United States. Proceedings, Thirty-Second Work Geotherm Reserv Eng 2007. 2007.
[4] Rybach L. "The Future of Geothermal Energy" and Its Challenges. World Geotherm Congr 2010:1–4.
[5] Winsloe R, Richter A, Vany J. The Emerging (and Proven) technologies that could finally make geothermal scalable. Proc. World Geotherm. Congr. 2020;2:1–11.
[6] Polsky Y, Blankenship D, Mansure AJ, Swanson RJ, Capuano LE. In: Enhanced geothermal systems well construction technology evaluation; 2009. https://doi.org/10.1190/1.3255790.
[7] Lu SM. A global review of enhanced geothermal system (EGS). Renew Sustain Energy Rev 2018;81:2902–21. https://doi.org/10.1016/j.rser.2017.06.097.
[8] Olasolo P, Juárez MC, Morales MP, Damico S, Liarte IA. Enhanced geothermal systems (EGS): a review. Renew Sustain Energy Rev 2016;56:133–44. https://doi.org/10.1016/j.rser.2015.11.031.
[9] Pan SY, Gao M, Shah KJ, Zheng J, Pei SL, Chiang PC. Establishment of enhanced geothermal energy utilization plans: barriers and strategies. Renew Energy 2019;132:19–32. https://doi.org/10.1016/j.renene.2018.07.126.
[10] Schulz S-U. Investigations on the improvement of the energy output of a closed loop geothermal system (CLGS). Technische Universität Berlin; 2008.
[11] Hu Z, Xu T, Feng B, Yuan Y, Li F, Feng G, et al. Thermal and fluid processes in a closed-loop geothermal system using CO2 as a working fluid. Renew Energy 2020;154:351–67. https://doi.org/10.1016/j.renene.2020.02.096.
[12] Amaya A, Scherer J, Muir J, Patel M, Higgins B. GreenFire energy closed-loop geothermal demonstration using supercritical carbon dioxide as working fluid. In: 45th Work. Geotherm. Reserv. Eng.,; 2020. p. 1–19.
[13] Eavor. Eavor-Loop. <https://eavor.com/about/eavor-loop-basics>; 2020.
[14] Yu H, Li Q, Sun F. Numerical simulation of CO2 circulating in a retrofitted geothermal well. J Pet Sci Eng 2019;172:217–27. https://doi.org/10.1016/j.petrol.2018.09.057.
[15] Bu X, Ma W, Li H. Geothermal energy production utilizing abandoned oil and gas wells. Renew Energy 2012;41:80–5. https://doi.org/10.1016/j.renene.2011.10.009.
[16] Ebrahimi M, Torshizi SEM. Optimization of power generation from a set of low-temperature abandoned gas wells, using organic Rankine cycle. J Renew Sustain Energy 2012:4. https://doi.org/10.1063/1.4768812.
[17] Oldenburg CM, Pan L, Muir MP, Eastman AD, Higgins BS. Numerical simulation of critical factors controlling heat extraction from geothermal systems using a closed-loop heat exchange method. In: 41st Work Geotherm. Reserv. Eng.; 2016. p. 1–8.
[18] Blackwell D, Richards M, Frone Z, Batir J, Ruzo A, Dingwall R, et al. Temperature-at-depth maps for the conterminous U. S. and geothermal resource estimates. Trans - Geotherm Resour Counc 2011;35(2):1545–50.
[19] Kozlovsky Y. The World's deepest well. Sci Am 1984;251:98–105.
[20] Emmermann R, Lauterjung J. The German continental deep drilling program KTB: overview and major results. J Geophys Res Solid Earth 1997:102. https://doi.org/10.1111/j.1365-246X.1991.tb00816.x.
[21] Gupta VP, Yeap AHP, Fischer KM, Mathis RS, Egan MJ. Expanding the extended reach envelope at Chayvo Field, Sakhalin Island (Russian). Soc Pet Eng - SPE Annu Casp Tech Conf Exhib 2014;1:1–23.
[22] Ma T, Chen P, Zhao J. Overview on vertical and directional drilling technologies for the exploration and exploitation of deep petroleum resources. Geomech Geophys Geo-Energy Geo-Resources 2016;2:365–95. https://doi.org/10.1007/s40948-016-0038-y.
[23] Rosneft. The World's Longest Well Was Drilled in Sakhalin; 2017.
[24] Shadravan A, Amani M. HPHT 101-what petroleum engineers and geoscientists should know about high pressure high temperature wells environment. Energy Sci Technol 2012;4:36–60. https://doi.org/10.3968/j.est.1923847920120402.635.
[25] Rehm B, Schubert J, Haghshenas A, Paknejad AS, Hughes J. Managed Pressure Drilling. Elsevier; 2008.
[26] Sun F, Yao Y, Li G. Literature review on a U-shaped closed loop geothermal energy development system. Energy Sources, Part A Recover Util Environ Eff 2020;42:2794–806. https://doi.org/10.1080/15567036.2019.1618990.
[27] Sun F, Yao Y, Li G, Li X. Geothermal energy development by circulating CO2 in a U-shaped closed loop geothermal system. Energy Convers Manag 2018;174:971–82. https://doi.org/10.1016/j.enconman.2018.08.094.
[28] Sun X, Wang Z, Liao Y, Sun B, Gao Y. Geothermal energy production utilizing a U-shaped well in combination with supercritical CO2 circulation. Appl Therm Eng 2019;151:523–35. https://doi.org/10.1016/j.applthermaleng.2019.02.048.

[29] Song X, Shi Y, Li G, Shen Z, Hu X, Lyu Z, et al. Numerical analysis of the heat production performance of a closed loop geothermal system. Renew Energy 2018; 120:365–78. https://doi.org/10.1016/j.renene.2017.12.065.
[30] Cheng WL, Huang YH, Lu DT, Yin HR. A novel analytical transient heat-conduction time function for heat transfer in steam injection wells considering the wellbore heat capacity. Energy 2011;36:4080–8. https://doi.org/10.1016/j.energy.2011.04.039.
[31] Ramey HJ. Wellbore Heat Transmission. J Pet Technol 1962;14:427–35. https://doi.org/10.2118/96-pa.
[32] Fallah A, Gu Q, Ma Z, Karimi Vajargah A, Chen D, Ashok P, et al. An integrated thermal and multi-phase flow model for estimating transient temperature dynamics during drilling operations. SPE/IADC Drill. In: Conf., vol. 2019; 2019. https://doi.org/10.2118/194083-ms.
[33] Fallah A, Gu Q, Ma Z, Vajargah AK, Chen D, Ashok P, et al. Temperature dynamics and its effects on gas influx handling during managed pressure drilling operations. J Nat Gas Sci Eng 2020. https://doi.org/10.1016/j.jngse.2020.103614.
[34] Kabir CS, Hasan AR, Kouba GE, Ameen MM. Determining circulating fluid temperature in drilling, workover, and well-control operations. SPE Drill Complet 1996;11:74–8. https://doi.org/10.2118/24581-pa.
[35] Petersen J, Rommetveit R, Tarr BA. Kick with lost circulation simulator, a tool for design of complex well control situations. In: SPE - Asia Pacific Oil Gas Conf.; 1998. p. 25–33. https://doi.org/10.2523/49956-ms.
[36] Ma Z, Karimi Vajargah A, Ambrus A, Ashok P, Chen D, van Oort E, et al. Multi-phase well control analysis during managed pressure drilling operations. In: Proc. - SPE Annu. Tech. Conf. Exhib., Society of Petroleum Engineers; 2016. https://doi.org/10.2118/181672-ms.
[37] Ahmed R, Miska S. Advanced Wellbore Hydraulics. In: Aadnoy Bernt S, editor. Advaned drilling and well technology. USA Society of Petroleum Engineers. SPE; 2009.
[38] Nellis G, Klein S. Heat transfer. Cambridge University Press; 2009.
[39] Moran MJ, Shapiro HN, Boettner DD, Bailey MB. Fundamentals of engineering thermodynamics. John Wiley & Sons; 2010.
[40] Lemmon EW, McLinden MO, Friend DG. Thermophysical Properties of Fluid Systems. In: Linstrom PJ, Mallard WG, editors. NIST Chem. WebBook, NIST Stand. Ref. Database Number 69. National Institute of Standards and Technology; 2018. https://doi.org/10.18434/T4D303.
[41] Evje S, Fjelde KK. Relaxation schemes for the calculation of two-phase flow in pipes. Math ComputModel 2002;36:535–67. https://doi.org/10.1016/S0895-7177(02)00182-6.
[42] Zoback MD. Reservoir Geomechanics; 2010. https://doi.org/10.1017/CBO9780511586477.
[43] Whittington AG, Hofmeister AM, Nabelek PI. Temperature-dependent thermal diffusivity of the Earth's crust and implications for magmatism. Nature 2009;458:319–21. https://doi.org/10.1038/nature07818.
[44] Eppelbaum L, Kutasov I, Pilchin A. In: Applied Geothermics. Springer Berlin Heidelberg; 2014. https://doi.org/10.1007/978-3-642-34023-9.
[45] Adams BM, Kuehn TH, Bielicki JM, Randolph JB, Saar MO. On the importance of the thermosiphon effect in CPG (CO2 plume geothermal) power systems. Energy 2014;69:409–18. https://doi.org/10.1016/j.energy.2014.03.032.
[46] Gu Q, Fallah A, Ambrus A, Ma Z, Chen D, Ashok P, et al. A switching MPD controller for mitigating riser gas unloading events in offshore drilling. SPE Drill Complet 2020. https://doi.org/10.2118/194163-PA. Preprint:17.
[47] Gu Q, Fallah A, Feng T, Bakshi S, Chen D, Ashok P, et al. A novel dilution control strategy for gas kick handling and riser gas unloading mitigation in deepwater drilling. J Pet Sci Eng 2020;196:107973. https://doi.org/10.1016/j.petrol.2020.107973.
[48] Kinik K, Gumus F, Osayande N. Automated dynamic well control with managed-pressure drilling: a case study and simulation analysis. SPE Drill Complet 2015;30:110–8. https://doi.org/10.2118/168948-PA.